# TOTAL AND ELASTIC CROSS-SECTIONS AT HIGH ENERGY

R. L. Loveless
University of Michigan
Ann Arbor, MI 48104

## 1. INTRODUCTION

I will try to summarize the progress made in the last 2 years in the field of total and elastic cross-sections at high energy.[1] Most of my information comes from published data, except for my own group's data, so any mistakes in this report are due solely to me. I will discuss the total cross-sections first concentrating on the energy dependence and interrelationships between various cross-sections. Then I will examine the elastic results, concentrating on the slope near $|t| \sim .2$ $(GeV/c)^2$ and its energy dependence. I will conclude with a discussion of the pp cross-section near the observed dip at $|t| \sim 1.4$ $(GeV/c)^2$.

## 2. TOTAL CROSS-SECTIONS

### 2.1 Status in 1972

Two years ago the very first data from Serpukhov, the CERN ISR, and Fermilab were available.[2] At that time, the data from Serpukhov[3] was the most precise. It showed the $\pi^{\pm}$, $K^{\pm}$, and $p^{\pm}$ total cross-sections on protons and neutrons up to a laboratory momentum ($p_{Lab}$) of 60 (GeV/c). This data showed that all the cross-sections had reached an energy-independent value with the exception of $K^+p$ which was rising and the $p^-p$ and $p^-n$ which were falling.

The ISR data on pp only, of course, went up to a laboratory momentum of 1500 (GeV/c) but had quite large error bars ($\sim$1-2 mb) because of the preliminary nature of the experiments. The Fermilab data (mostly early bubble chamber data) was also imprecise ($\sim$1 mb). These high energy results (pp only) showed no deviation from the Serpukhov result of a constant pp total cross-section and it was believed that asymtopia may have been reached.

### 2.2 Recent Data on Protons

The major progress in the last two years has been the increased precision of the ISR data and the introduction of data from the high-precision Fermilab-Rockefeller-Brookhaven (FRB) counter experiment.[4]

Figure 1 shows the present state of the pp total cross-section. The Serpukhov and the FRB total cross-sections were obtained with the standard transmission counter technique. Briefly, this method consists of measuring the number of particles scattered into smaller and smaller $|t|$ regions and then extrapolating to obtain $d\sigma/dt$ at $t = 0$, the well-known optical point. In both experiments, the form used to fit the t distribution was:

$$\left(\frac{d\sigma}{dt}\right)_i = \left(\frac{d\sigma}{dt}\right)_o \cdot \exp(bt_i + ct_i^2). \qquad (1)$$

The t range was almost identical for the two extrapolations; $.013 < |t| < .064$ $(GeV/c)^2$. The total cross-section can be calculated by the following formula:

$$\sigma^2_{total} = \frac{16\pi}{1+\rho^2} \cdot \left(\frac{d\sigma}{dt}\Big|_o\right) \qquad (2)$$

where $\rho$ is the ratio of the real to the imaginary part of the elastic scattering amplitude.

The FRB data matches the older Serpukhov data well at 50 (GeV/c) and shows an increase in the pp total cross-section of (.76 ± .10) mb from 50 - 200 (GeV/c).

Both ISR groups, CERN-Rome[5] and Pisa-Stonybrook,[6] have significantly increased their precision to obtain an error bar of less than 1 mb. I will briefly describe the ISR methods also, since they are not the standard transmission method.

The CERN-Rome group detects both protons from elastic pp collisions and forms the t-distribution similar to the transmission experiments. Then the t-distribution is extrapolated to $t = 0$ and the same formula (2) is used to obtain $\sigma_{total}$. Because they are at a storage ring, they must use the Van der Meer method to determine the luminosity and, hence, the normalization. The transmission experiments simply count the number of beam particles. To check the Van der Meer method, they also determined the normalization from the Coulomb-nuclear interference at very small t's. The two methods agree very well. CERN-Rome state a 3% scale uncertainty.

The Pisa-Stonybrook group uses an orthogonal approach to the problem. Instead of concentrating only on small angle scattering, they actually measure all the scattering events outside the small angle scattering by surrounding the interaction region with scintillation counters and using a loose trigger. Then they correct the measured cross-section for the small angle events they miss to obtain the total pp cross-section. This method has the virtue of being independent of the

optical theorem and insensitive to the form of the extrapolation to t = 0.

The ISR experiments are consistent and show a rise in the pp total cross-section of (3.9 ± .8) mb as $p_{Lab}$ increases from 280 to 1500 (GeV/c). This rise is consistent with either a lns or a $\ln^2 s$ dependence.

While the ISR has a tremendous energy advantage, the transmission-type experiment can measure more accurately and can study $\pi^{\pm}p$, $K^{\pm}p$, and $p^{-}p$ total cross-sections for each of the 6 particles.
As can be seen (Fig. 1), the $\bar{p}p$ cross-section falls and is approaching the pp cross-section as the energy increases.

The $\pi^{+}p$ and $\pi^{-}p$ cross-sections are shown in Fig. 2. Amazingly, considering the presumed approach to asymtopia, the $\pi^{+}p$ and $\pi^{-}p$ cross-sections both reach a minimum and then rise as the energy is increased! The $\pi^{-}p$ remains larger than the $\pi^{+}p$ cross-section but the difference is decreasing.

The $K^{+}p$ and $K^{-}p$ cross-sections are shown in Fig. 3. Again, surprizingly, the $K^{-}$ cross-section reaches a minimum and then rises! The $K^{+}p$ cross-section, which had been rising at Serpukhov energies continues to rise, decreasing the $K^{-}$-$K^{+}$ difference.

## 2.3 Recent Neutron Data

The standard transmission experiments can also be done with deuterium. After applying the Glauber corrections, the neutron cross-sections can be obtained. The formula for the Glauber correction used is:[7]

$$\sigma_d = \sigma_p + \sigma_n - \delta \tag{3}$$

where the Glauber correction $\delta$ is:

$$\delta = \frac{\langle r^{-2} \rangle}{4\pi} \sigma_p \sigma_n [1 - \rho_p \rho_n] \tag{4}$$

$\langle r^{-2} \rangle$ represents the mean inverse square separation of the neutron and the proton in the deuteron. There is some question presently whether the $\langle r^{-2} \rangle$ is energy independent and/or particle-type independent.[8] Both the Serpukhov and FRB groups fit $\langle r^{-2} \rangle$ at each energy using the $\pi^{\pm}d$ and $\pi^{\pm}p$ data. The values are relatively consistent with each other and with the preferred deuteron wave function calculations at about (.035 ± .005) ($^1$/mb).

The $p^{\pm}n$ cross-sections are shown in Fig. 4. The pn cross-section rises very slightly from 50 - 200 (GeV/c), while the $p^{-}n$ cross-section falls significantly to

150 (GeV/c) and then remains constant or slightly increases. The statistical error at large $p_{Lab}$ is large because of the low $p^-$ beam intensity. The $K^{\pm}n$ cross-sections are shown in Fig. 5 and are very similar to $K^{\pm}p$. The $K^-n$ cross-section seems to reach a minimum near 50 (GeV/c) and then increases about 2½% by $p_{Lab}$ ∿ 200 (GeV/c).

The $\pi^{\pm}n$ cross-sections are not shown because they should equal the $\pi^{\mp}p$ cross-sections by charge symmetry. This symmetry is assumed in calculating $\langle r^{-2} \rangle$. The validity of this assumption is borne out by the fact that $\pi^+d$ and $\pi^-d$ cross-sections are equal.

Table I summarizes the FRB results and Table II gives the latest published ISR results.

### 2.4 Relations between Total Cross-sections

Now that all six particle total cross-sections have been measured up to 200 (GeV/c), the relations between the cross-sections derived from Regge pole, SU(3), and quark models can be examined.[9] The simplest quark prediction is:

$$\sigma(NN) \sim \frac{3}{2} \sigma(\pi N) \tag{5}$$

which results from simple quark counting. This relation was not well satisfied at Serpukhov energies and the new data shows only a weak trend towards agreement. (See Fig. 8).

The Johnson-Treiman relations are derived from SU(6) symmetry and state that:

$$\frac{\Delta\sigma(K^{\pm}p)}{2} \sim \Delta\sigma(\pi^{\pm}p) \sim \Delta\sigma(K^{\pm}n) \tag{6}$$

These relations seem to be in agreement to the 5-10% level.[10]

The second Pomeranchuk theorem states that the cross-section for a particle and its anti-particle should become equal as the energy is increased. Regge theory predicts that this particle-anti-particle difference should decrease as a power of $p_{Lab}$ (or equivalently s):

$$\Delta\sigma = Ap_{Lab}^{-n} \tag{7}$$

Figure 6 shows the difference between $p^+$ and $p^-$ cross-sections plotted versus $p_{Lab}$. The new results, in fact, continue to exhibit this type of power law falloff observed at Serpukhov energies. Figure 7 shows a similar plot for K's and π's. In all cases the new results

continue to lie along the power law falloff curve determined from the Serpukhov data. Table III summarizes the FRB values for n.

In the Regge-pole model, the pion-nucleon difference is due only to the ρ pole term. The kaon-proton difference is due to the sum of the ω, ρ terms and the kaon-neutron difference is due to the difference of the ω and ρ terms. Thus, the ρ and ω terms can be separately determined for the kaon-nucleon system.

The p-nucleon system is similar to the kaon system and the ρ and ω terms can be separated. The results of these calculations is shown in Table IV. The numerical values are from the Serpukhov data. The continued falloff of the cross-sections observed at Fermilab means that ρ and ω universality which was valid at Serpukhov energies continues to be a valid concept as $p_{Lab}$ increases.

The fact that $\Delta\sigma(KN)$ decreases as $p_{Lab}$ increases implies that the $K^o_L$ regeneration amplitude must also decrease. The San Diego-Chicago-Wisconsin group[11] at Fermilab has measured the $K^o_L$ regeneration cross-section on carbon directly. (Fig. 9).

The FRB data on total cross-sections give the value of the imaginary part of the $K^o p$, $K^o n$, $\bar{K}^o p$, and $\bar{K}^o n$ amplitudes at $t = 0$ if isotopic spin invariance is assumed. This is then combined with an optical model of carbon, some assumption of the real part of each particular amplitude, and a fixed final phase of $\pi/4$ to yield the values shown. These values are in good agreement with the actual regeneration measurements of the SD-C-W group. The result is that $|f-\bar{f}|/k$ exhibits a $p_{Lab}^{-\frac{1}{2}}$ falloff which is a continuation of the lower energy and Serpukhov trend.

The group is collecting more data and should significantly improve the accuracy of their values by the end of the year. They now are using a $CH_2$ target and expect to measure regeneration from a hydrogen target in the near future. In addition to the regeneration measurements, they have measured the $K^o_L$ total cross-section on carbon and obtain a value of (178 ± 10) mb.

## 3. ELASTIC SCATTERING

### 3.1 Introduction

Now I will turn my attention to elastic scattering. The basic shape of all elastic scattering cross-sections is a large forward peak with a very sharp falloff, followed by a small sometimes structured intermediate region, followed by a small backward peak. No new data, to my knowledge, has appeared since the Batavia

conference on backward peaks, so I will not discuss it here.

### 3.2 Small |t| Region

First, I will consider the very small |t| region; i.e., $|t| < .01$ (GeV/c)$^2$. Since this region involves the Coulomb term whose amplitude and phase are well-known, it is used to determine $\rho$, the real/imaginary ratio for the nuclear scattering amplitude near t = 0. A typical graph is shown in Fig. 10. The functional form of $d\sigma/dt$ in the interference region is:

$$\frac{d\sigma}{dt} = K_1 \frac{G^4(t)}{t^2} - K_2(\rho+\alpha\phi)\frac{G^2(t)}{|t|}\sigma_\tau e^{bt/2} + K_3(1+\rho^2)\frac{\sigma_\tau^2}{4\pi} e^{bt} \quad (8)$$

where $K_1$-$K_3$ are constants and $\alpha\phi$ is the phase of the Coulomb amplitude. As I have already mentioned, the CERN-Rome group has measured this as part of determining the total cross section. In addition, a Fermilab experiment at the internal target area has measured the recoil proton from elastic scattering at very small |t| using a hydrogen jet and solid-state detectors.[12] The results (Fig. 11) show that $\rho$, the real/imaginary ratio, which had been approximately $-\frac{1}{3}$ at about 5 GeV/c slowly and continually increases towards zero throughout the 5-500 GeV/c range. The highest energy points indicate that $\rho$ has become positive at about $p_{Lab} \sim 300$ (GeV/c). The CERN-Rome group cannot determine $\rho$ above $p_{Lab} \sim 500$ (GeV) because they cannot position their counters close enough to observe the Coulomb-nuclear interference region. Some dispersion relations using spin independent amplitudes indicate that a rising $\sigma_{Total}$ will lead to a positive $\rho$.

### 3.3 Intermediate |t| Region

In the diffraction region, the major new data is from the Fermilab experiment conducted by a Michigan-Argonne-Indiana-Fermilab collaboration[13] of which I am a member. We have collected data on $\pi^\pm p$, $K^\pm p$, and $p^\pm p$ at both 100 and 200 (GeV/c) over a range of |t| from .07 to $\sim$ 1.0. At 200, the $K^-p$ and $p^-p$ distributions do not contain enough data to be statistically significant and, thus, are not presented here. Briefly, each beam particle is tagged by 2 differential and one threshold Cherenkov counters into $\pi$, K, or p. The forward scattered particle's angle and momentum are measured by wire spark chambers in a magnetic spectrometer while the angle of the recoil proton is also measured with wire spark chambers.

An elastic event is defined by (1) correct $MM^2$ for the recoil proton calculated using only the forward particle, (2) coplanarity and (3) opening angle. These three criterion essentially eliminate the inelastic background. Figure 12 shows the $p^+p$ and $p^-p$ data. While $p^-p$ is consistent with a purely exponential fall-off, the $p^+p$ exhibits a definite departure. The straight line drawn through the data is the best purely exponential fit for the data between $.07<|t|<.30$ $(GeV/c)^2$.

The $\pi^\pm p$ data is shown in Fig. 13. The data here also shows a break or at least a curvature from the purely exponential fit at about $|t| \sim .3$ $(GeV/c)^2$. Figure 14 shows the $K^\pm p$. Where the data is statistically good, the K's clearly exhibit curvature beyond $|t| \sim .3$ $(GeV/c)^2$.

The energy dependence of the $p^\pm p$ slopes at $|t| \sim .2$ $(GeV/c)^2$ is shown in Fig. 15. The pp slope falls along the interpolation between low energy and ISR results. (N. B. there is no Serpukhov data on positive particles). The $p^-p$ slope at 100 (GeV/c) indicates that the $\bar{p}p$ and $p^+p$ slopes have become essentially equal. The low intensity of $\bar{p}$'s at 200 (GeV/c) unfortunately prevents us from determining an accurate slope.

The energy dependence of the slope parameters for the mesons is shown in Fig. 16. The $\pi^\pm p$ slopes increase smoothly from the low energy values through Serpukhov energies to about 100 (GeV/c). From 100 to 200 (GeV/c), the slopes seem to be constant or perhaps increasing very slowly. The $K^-p$ slope seems to increase smoothly and is approximately equal to the $\pi^+p$ slope and somewhat lower than the $\pi^-p$ slope. The $K^+p$ slope which had the smallest value at low energy increases most rapidly until it reaches a value of $\sim 8$ $(GeV/c)^{-2}$ at 200 (GeV/c).

I should add a word of caution at this point. Our data is not published and should be considered preliminary. In particular, the overall normalization has not been completed yet. This will not affect the slopes significantly since the acceptance in t is very flat, but it will directly affect the optical point determined from our data.

We hope to significantly improve the K slope accuracy at 200 (GeV/c) and fill in a 50 (GeV/c) point for all 6 particles.

The general picture of elastic slope data is that all diffraction width are decreasing (shrinking) with the exception of $p^-p$ which is increasing (anti-shrinking). The rate of shrinkage seems to diminish or perhaps vanish above a $p_{Lab} \sim 50$ (GeV/c). One popular theoretical idea for pp interactions, a naive geometrical model, pictures the size of the proton increasing

as $p_{Lab}$ increases according to ln $p_{Lab}$ (or ln s). This would lead to a total cross-section and a slope variation according to $\ln^2 p_{Lab}$ (or $\ln^2 s$), which is consistent with the data on total cross-section and not inconsistent with the slope measurements. The data on meson-proton slopes is very recent and no firm explanations have yet emerged.

### 3.4 High |t| Region

Another area of considerable interest is the high |t| region; the region beyond |t| = 1.0 $(GeV/c)^2$. At a |t| = 1.4 $(GeV/c)^2$, the ACGHT (Aachen-CERN-Geveva-Harvard-Turin) group at the ISR observes a sharp dip in pp elastic scattering.[14] At lower energies, there is a distinct break in the t-distribution at approximately the same t. This dip, which was reported 2 years ago at the Batavia conference, appears to be a classic example of a diffraction minimum and, thus, it has stimulated a great deal of theoretical work.

At the end of our group's latest data run, we tailor the trigger to enhance our data taking ability in the dip region at $p_{Lab}$ = 100 GeV/c. In approximately 3 days of running, we obtained the data shown in Fig. 17. No dip is apparent in our data but the statistical accuracy does not rule out a small dip ($\sim \frac{1}{2}$ as large as the ISR dip).

In an attempt to study the dip structure and its energy dependence, we hope to run later this month at 200 GeV/c with about a factor of 2-4 times the previous data taking rate. This is much closer to the lowest ISR energy ($p_{Lab}$ = 280 GeV/c) and so the dip should be more pronounced.

## 4. SUMMARY

To summarize the conclusions derived from total and elastic cross-sections in the last two years, several important points stand out:

(1) total cross-sections do not reach a constant, energy-independent value as energy increases, but seem to rise slowly above $p_{Lab} \sim 50$ GeV/c.
(2) the trends in the total cross-section data are such as to confirm theoretical predictions based on symmetry principles and Regge-pole models, but 10-20% discrepancies still exist.
(3) particle-anti-particle differences in total cross-sections continue to decrease according to a power law in $p_{Lab}$ (or s).

(4) all elastic t-distributions except $\bar{p}p$ show non-exponential behavior (curvature) in the region from $|t| \sim .1$ to $|t| \sim 1.0$ $(GeV/c)^2$ at 100 and 200 (GeV/c).

(5) the pp slopes around $|t| \sim .2$ $(GeV/c)^2$ at Fermilab energies fit a smooth curve between low energy and ISR values.

(6) the $p^-p$ slope ($\sim .2$ $(GeV/c)^2$) continues to decrease up to a $p_{Lab}$ of 100 GeV where it is approximately equal to the pp slope.

(7) the meson-proton slopes ($\sim .2$ $(GeV/c)^2$ continue to increase smoothly up to 100 GeV/c. Between 100 and 200 GeV, the slopes increase very little or remain constant.

(8) the particle-anti-particle slope differences (esp. K's) are decreasing.

## 5. ACKNOWLEDGEMENTS

I would like to thank the members of my experimental group who have all helped me understand this subject and prepare this paper.

## REFERENCES

1. For a statement of state of these subjects two years ago, see G. Giacomelli, XVI International Conference on High Energy Physics (Chicago-Batavia); Vol. 3; Planary Sessions Strong Interactions; p. 219. (1972).
2. See p. 279, 280 of Ref. 1.
3. S. P. Denisov, et al., Phys. Letters 36B, 528 (1971).
4. A. S. Carroll, et al., Data presented to Inter. Conf. at London, NAL-Pub-74/75-EXP (7100.104)(N. B. two papers), and to be published.
5. U. Amaldi, et al., Phy. Letters 44B, 112 (1973).
6. S. R. Amendolia, et al., Phys. Letters 44B, 119 (1973).
7. R. J. Glauber, Phys. Rev. 100, 242 (1955) and C. Wilkin, Phys. Rev. Letters 17, 561 (1966).
8. Yu. P. Gorin, et al., Sov. Journ. Nucl. Phys. 15, 530 (1972).
9. S. P. Denisov, et al., Nucl. Phys. B65, 1 (1973).
10. V. Barger, XVII International Conference on High Energy Physics in London, (Plenary Session).
11. E. I. Rosenberg, et al., abstract submitted to this conference and private communications.
12. V. Bartenev, et al., Phys. Rev. Letters 31, 1367 (1973).
13. C. W. Akerlof, et al., Abstract to this conference and submitted to XVII Inter. Conf. at London.
14. G. Barbiellini, et al., Phys. Letters 43B, 85 (1973).

LIST OF FIGURES

# Table I FRB Results

| | MOMENTUM (GeV/c) | | | | |
|---|---|---|---|---|---|
| | 50 | 100 | 150 | 200 | Momentum independent scale uncertainty |
| $\sigma_{pp}$ | 38.14±0.07 | 38.39±0.06 | 38.62±0.06 | 38.90±0.06 | ±0.5% |
| $\sigma_{pd}$ | 72.98±0.13 | 73.12±0.11 | 73.46±0.11 | 73.84±0.11 | ±0.6% |
| $\sigma_{\bar{p}p}$ | 43.86±0.11 | 42.04±0.09 | 41.72±0.18 | 41.54±0.29 | ±0.5% |
| $\sigma_{\bar{p}d}$ | 82.21±0.24 | 79.32±0.19 | 78.24±0.35 | 78.77±0.57 | ±0.6% |
| $\sigma_{pn}$ | 38.86±0.16 | 38.85±0.14 | 39.02±0.14 | 39.18±0.14 | ±1.5% |
| $\sigma_{\bar{p}n}$ | 43.69±0.30 | 42.22±0.23 | 41.32±0.44 | 42.09±0.71 | ±1.5% |
| $\sigma_{\bar{p}p} - \sigma_{pp}$ | 5.72±0.13 | 3.65±0.11 | 3.10±0.19 | 2.64±0.30 | |
| $\sigma_{\bar{p}d} - \sigma_{pd}$ | 9.23±0.28 | 6.20±0.22 | 4.78±0.37 | 4.92±0.58 | |
| $\sigma_{\bar{p}n} - \sigma_{pn}$ | 4.83±0.34 | 3.37±0.27 | 2.30±0.46 | 2.91±0.72 | |

| | MOMENTUM (GeV/c) | | | | |
|---|---|---|---|---|---|
| | 50 | 100 | 150 | 200 | Momentum independent Scale uncertainty |
| $\sigma_{\pi^-p}$ | 24.01±0.06 | 23.96±0.07 | 24.07±0.06 | 24.28±0.06 | ±0.5% |
| $\sigma_{\pi^-d}$ | 45.51±0.12 | 45.50±0.12 | 45.76±0.12 | 46.21±0.12 | ±0.6% |
| $\sigma_{\pi^+p}$ | 23.07±0.06 | 23.29±0.06 | 23.46±0.06 | 23.73±0.09 | ±0.5% |
| $\sigma_{\pi^+d}$ | 45.33±0.12 | 45.39±0.12 | 45.74±0.12 | 46.29±0.16 | ±0.6% |
| $\sigma_{K^-p}$ | 20.25±0.11 | 20.41±0.08 | 20.57±0.09 | 20.84±0.09 | ±0.5% |
| $\sigma_{K^-d}$ | 38.76±0.15 | 39.01±0.12 | 39.30±0.13 | 39.83±0.13 | ±0.6% |
| $\sigma_{K^-n}$ | 19.75±0.18 | 19.85±0.13 | 20.01±0.14 | 20.30±0.15 | ±0.7% |
| $\sigma_{K^+p}$ | 18.03±0.09 | 18.85±0.08 | 19.33±0.08 | 19.84±0.10 | ±0.5% |
| $\sigma_{K^+d}$ | 35.55±0.16 | 36.72±0.14 | 37.71±0.14 | 38.44±0.17 | ±0.6% |
| $\sigma_{K^+n}$ | 18.56±0.18 | 18.99±0.15 | 19.55±0.15 | 19.82±0.19 | ±0.7% |
| $\sigma_{\pi^-p} - \sigma_{\pi^+p}$ | 0.94±0.07 | 0.67±0.07 | 0.61±0.07 | 0.55±0.09 | |
| $\sigma_{K^-p} - \sigma_{K^+p}$ | 2.23±0.13 | 1.57±0.10 | 1.24±0.10 | 1.00±0.13 | |
| $\sigma_{K^-d} - \sigma_{K^+d}$ | 3.21±0.20 | 2.28±0.16 | 1.60±0.17 | 1.39±0.19 | |
| $\sigma_{K^-n} - \sigma_{K^+n}$ | 1.18±0.25 | 0.86±0.19 | 0.46±0.21 | 0.48±0.24 | |

**Table II Total pp Cross-sections ISR Results**

| | Equivalent $p_{Lab}$ | | | | |
|---|---|---|---|---|---|
| | 290 | 500 | 1070 | 1480 | Scale uncertainty |
| CERN-Rome | 39.1 ±.4 | 40.5 ±.5 | 42.5 ±.5 | 43.2 ±.6 | ±3% |
| Pisa-Stnybk | 39.30±.79 | 40.85±.82 | 42.57±.86 | 42.98±.84 | ±2% |

Table III

$\Delta\sigma = \sigma(x^-y) - \sigma(x^+y) = Ap_{Lab}^{-n}$

| x | y | n |
|---|---|---|
| $\pi$ | p | .60±.10 |
| K | p | .45±.07 |
| K | d | .39±.08 |
| p | p | .39±.04 |
| p | d | .43±.05 |

Table IV $\rho$, $\omega$ Universality

| | $\alpha$ in $s^{-(2\alpha-2)}$ |
|---|---|
| $\sigma_\rho(\pi N) = \frac{1}{2}\,\Delta\sigma(\pi p)$ | .67±.06 |
| $\sigma_\rho(KN) = \frac{1}{2}\,[\Delta\sigma(Kp) - \Delta\sigma(Kn)]$ | .63±.10 |
| $\sigma_\rho(NN) = \frac{1}{2}\,[\Delta\sigma(pp) - \Delta\sigma(pn)]$ | statistically consistent |
| $\sigma_\omega(KN) = \frac{1}{2}\,[\Delta\sigma(Kp) + \Delta\sigma(Kn)]$ | .44±.04 |
| $\sigma_\omega(NN) = \frac{1}{2}\,[\Delta\sigma(pp) + \Delta\sigma(pn)]$ | .43±.04 |

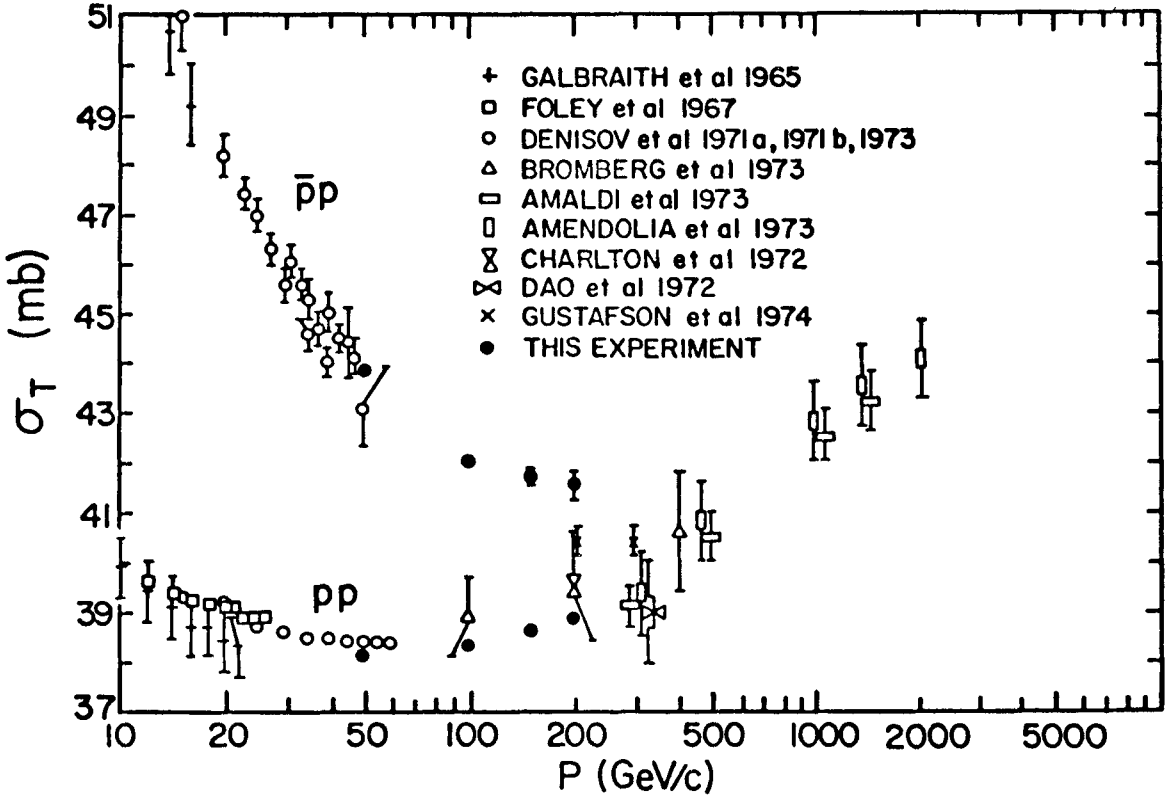


Fig. 1: pp, $\bar{p}p$ Total Cross-sections

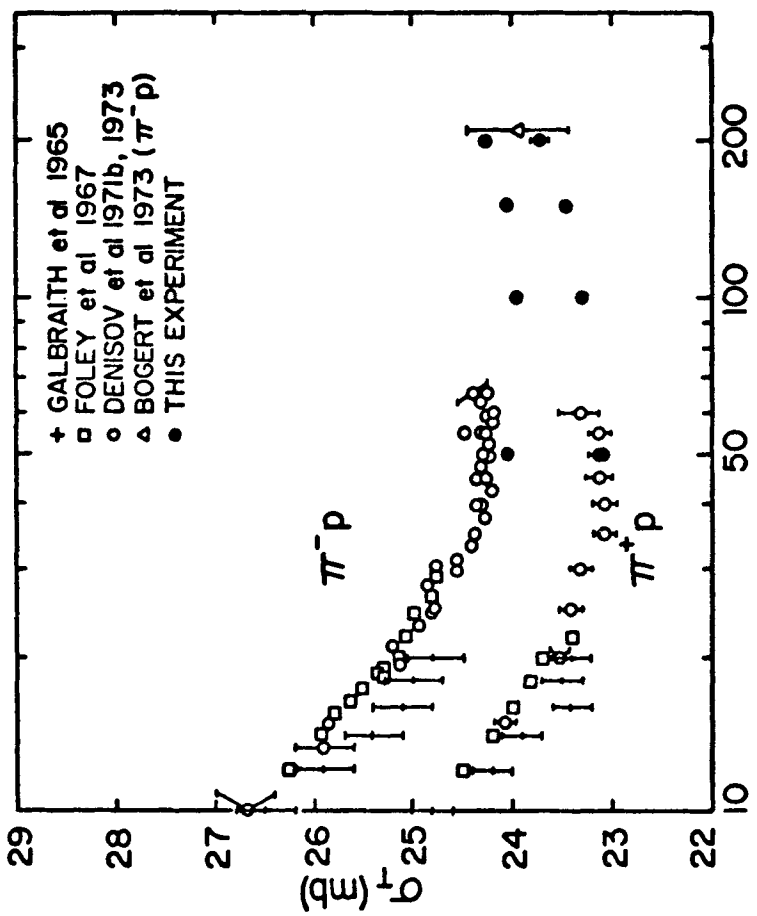


Fig. 2: $\pi^+p$, $\pi^-p$ Total Cross-sections

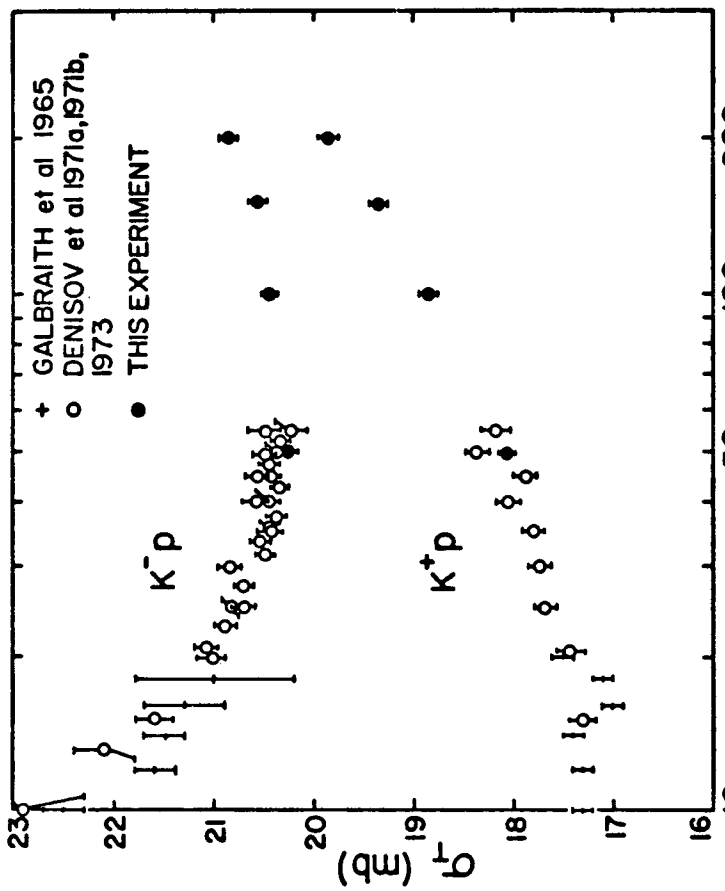


Fig. 3: $K^+p$, $K^-p$ Total Cross-sections

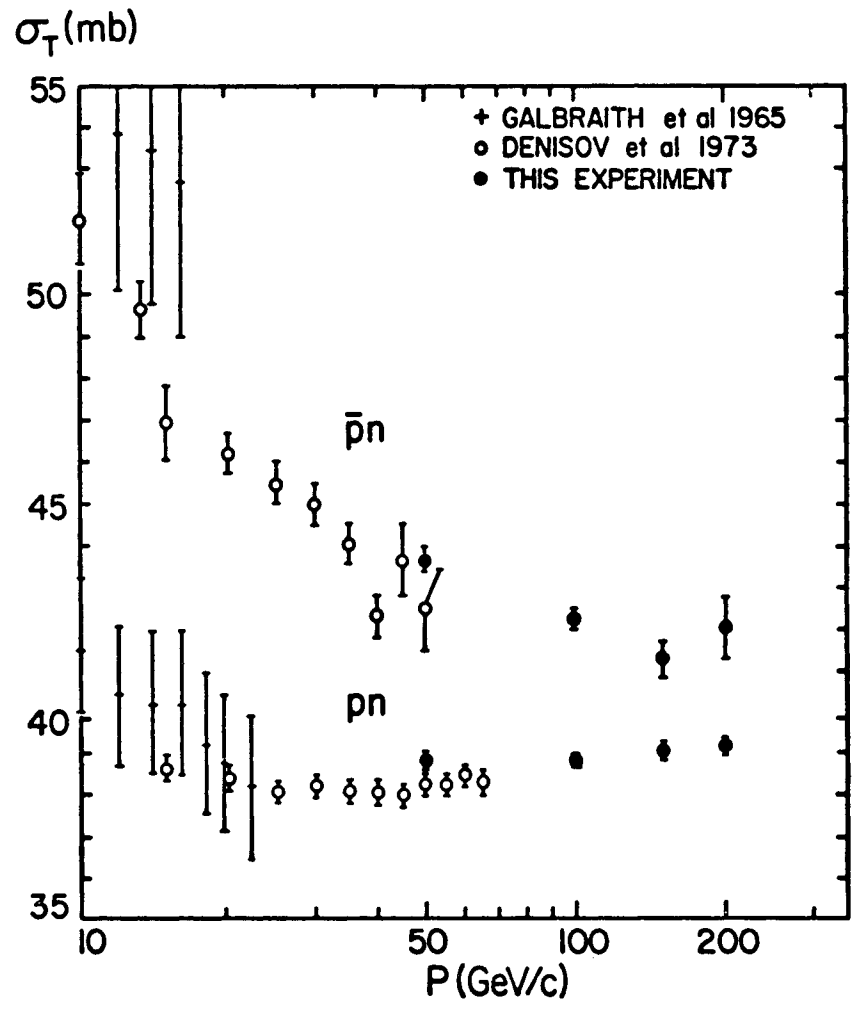


Fig. 4: pn, $\bar{p}n$ Total Cross-sections

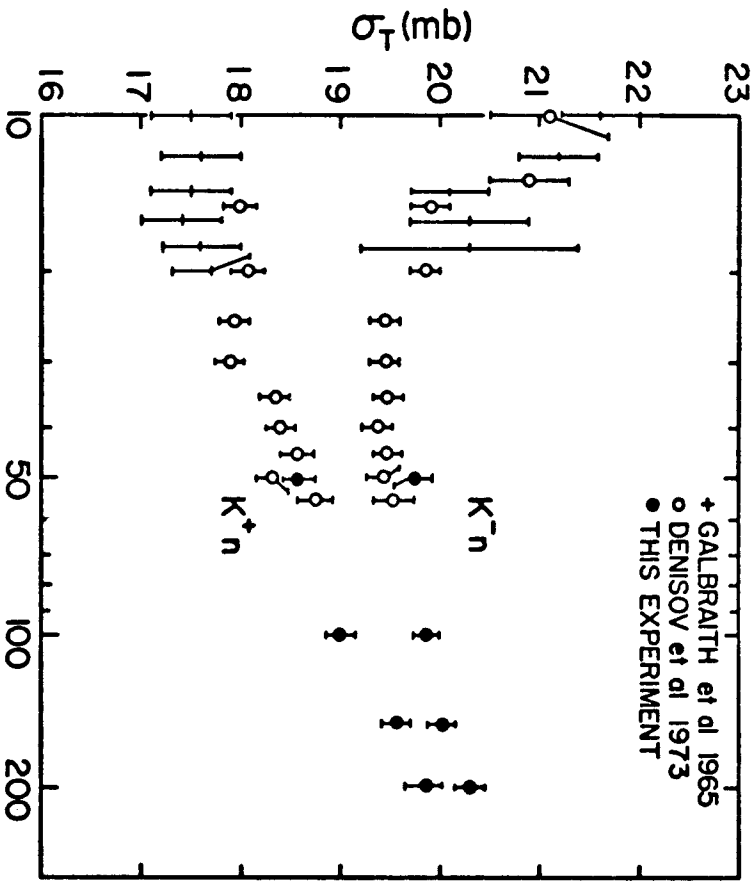


Fig. 5: $K^+n$, $K^-n$ Total Cross-section

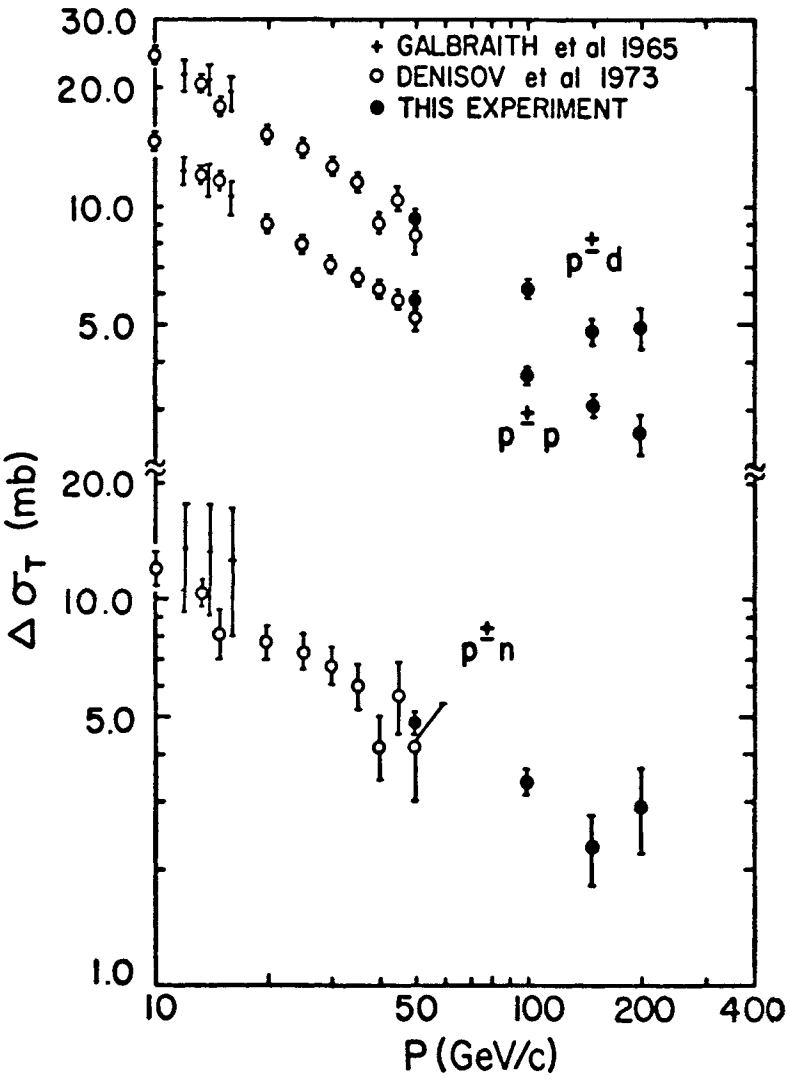


Fig. 6: $\Delta(p^{\pm}p)$ Total Cross-section Differences

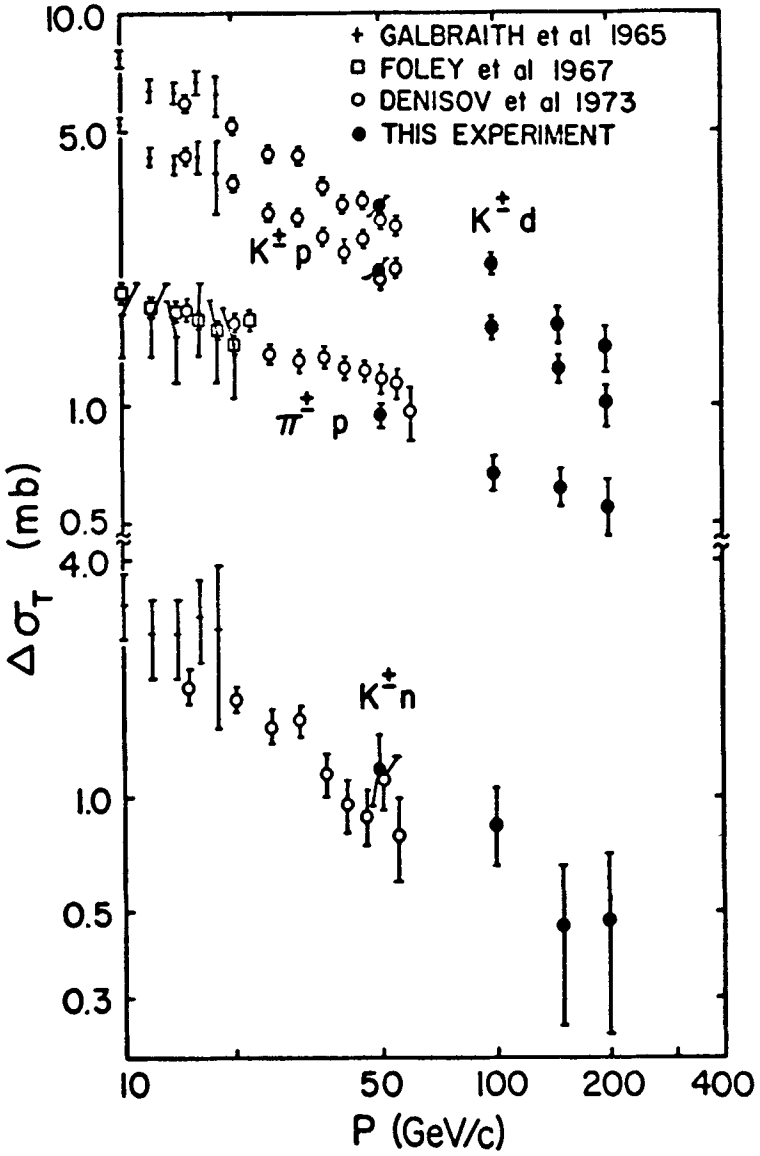


Fig. 7: $\Delta(\pi^{\pm}p)$ and $\Delta(K^{\pm}p)$ Total Cross-section Differences

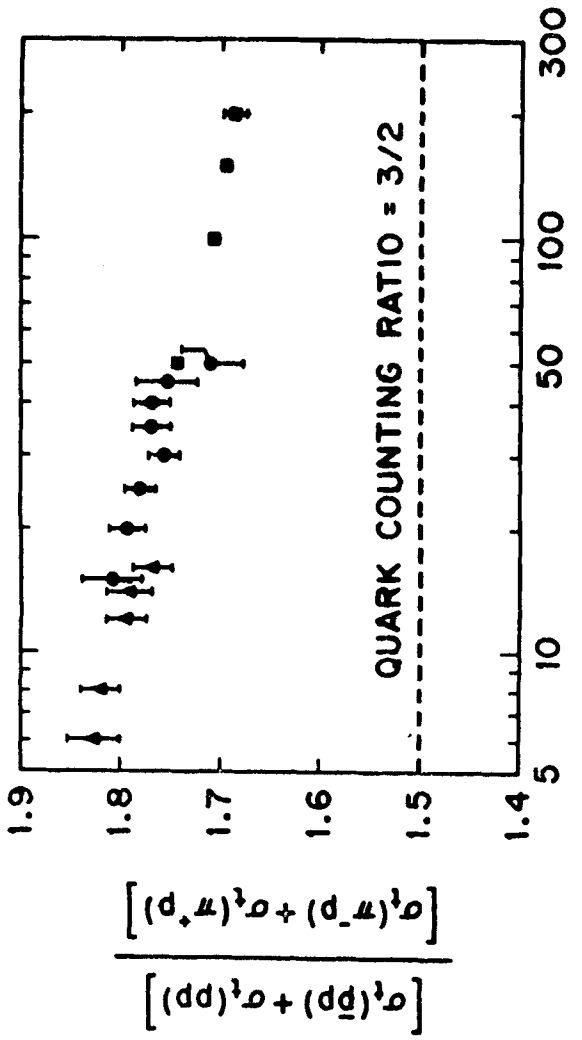


Fig. 8: Quark Counting Prediction

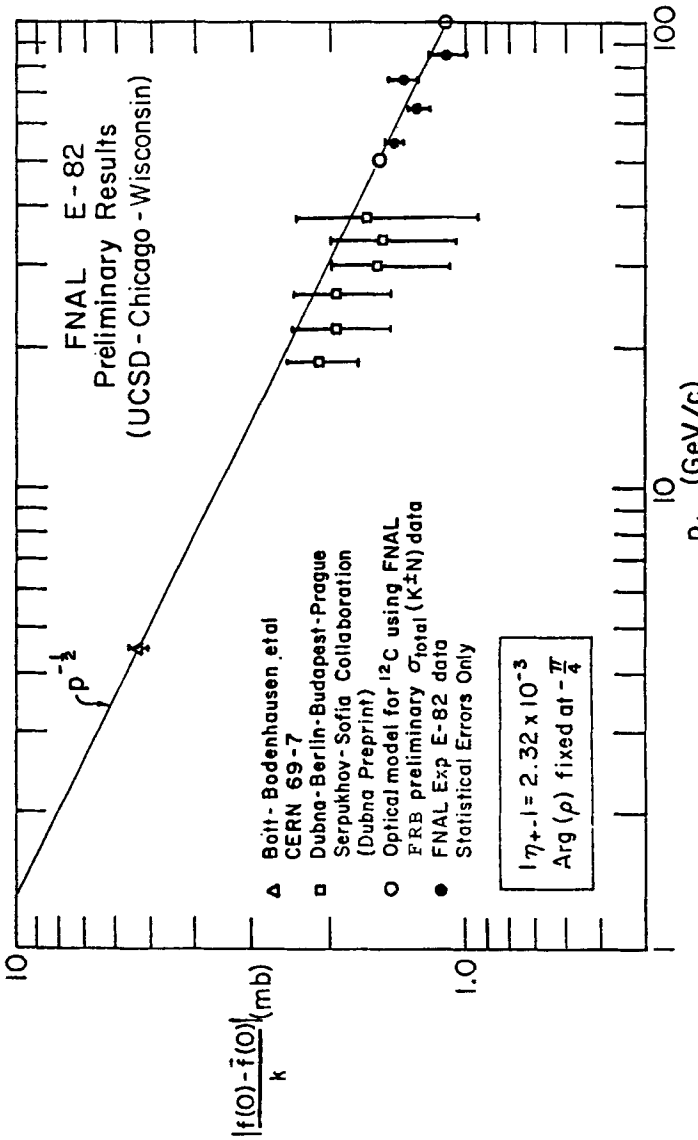


Fig. 9: $K^0$ Regeneration Amplitude

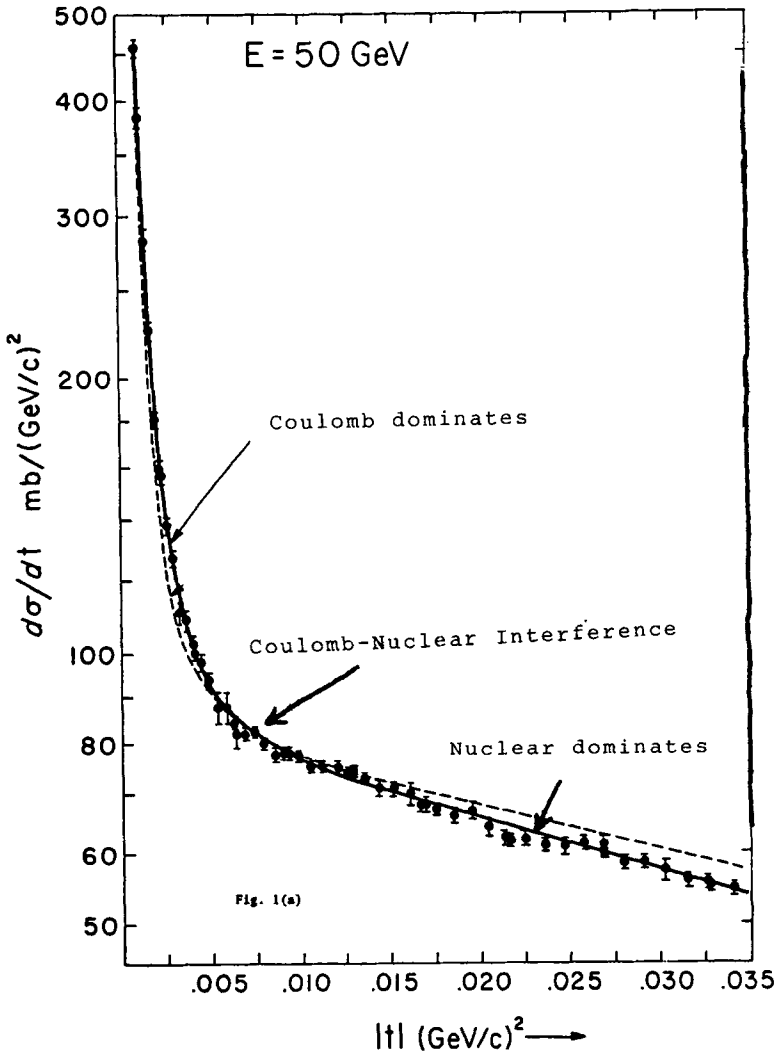


Fig. 10: Coulomb-Nuclear Interference

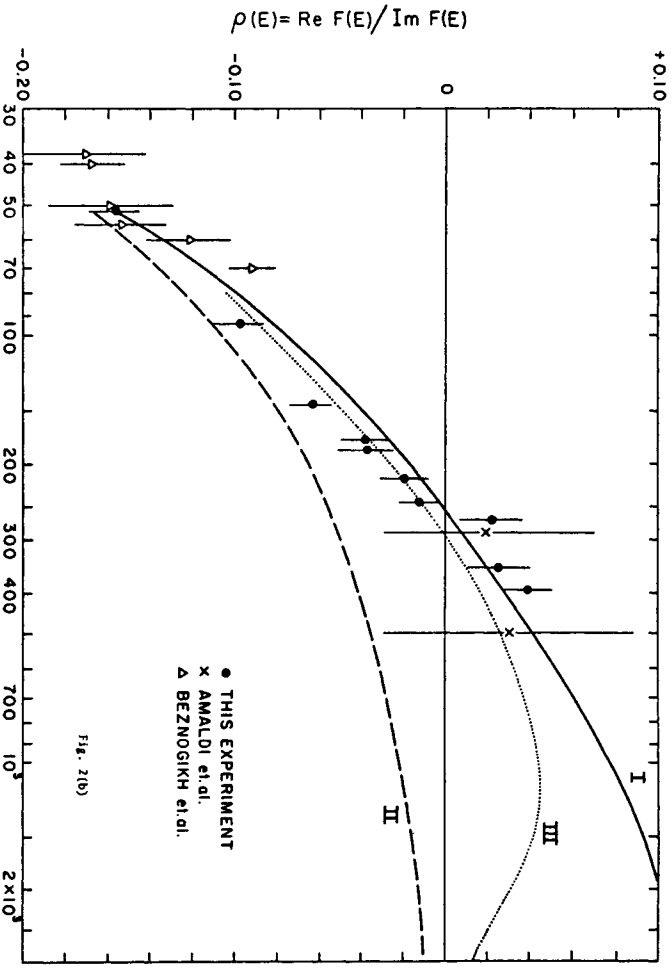


Fig. 11: ρ: Ratio of Real to Imaginary in pp Scattering

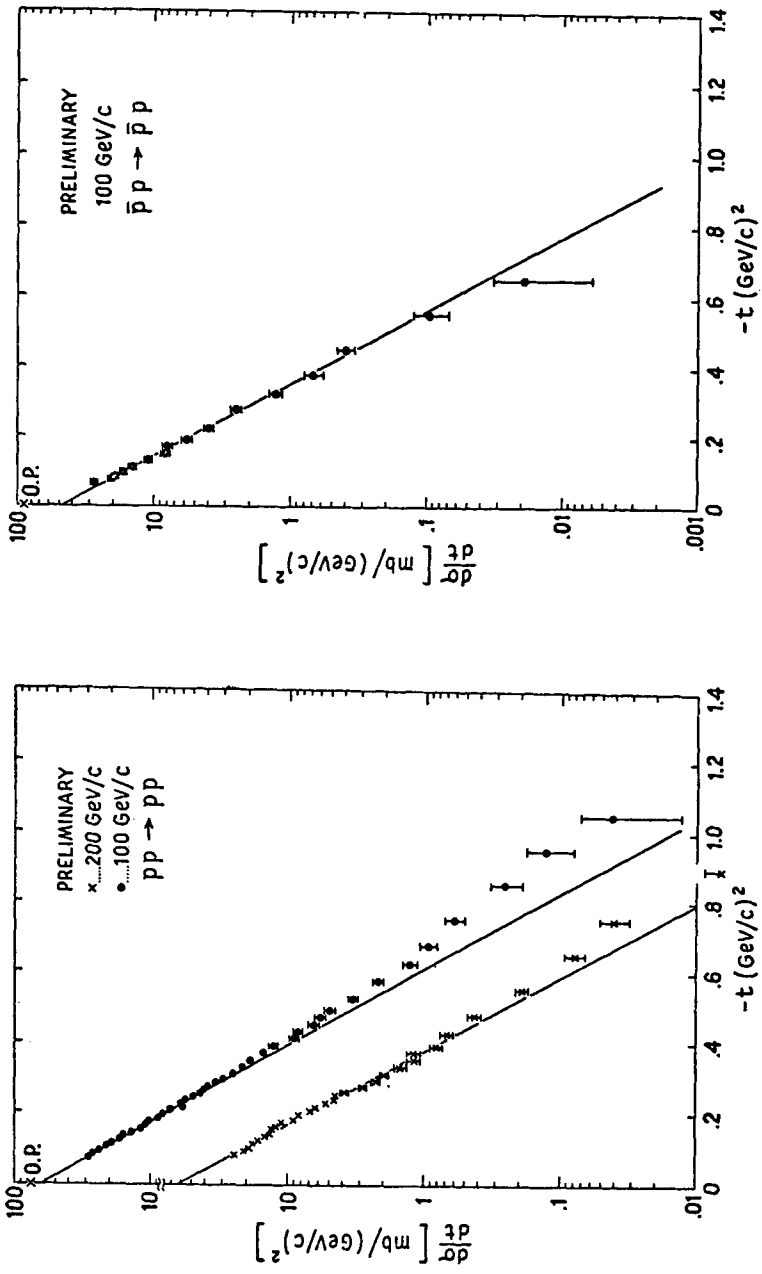


Fig. 12: Elastic Differential Cross-section $p^{\pm}p$

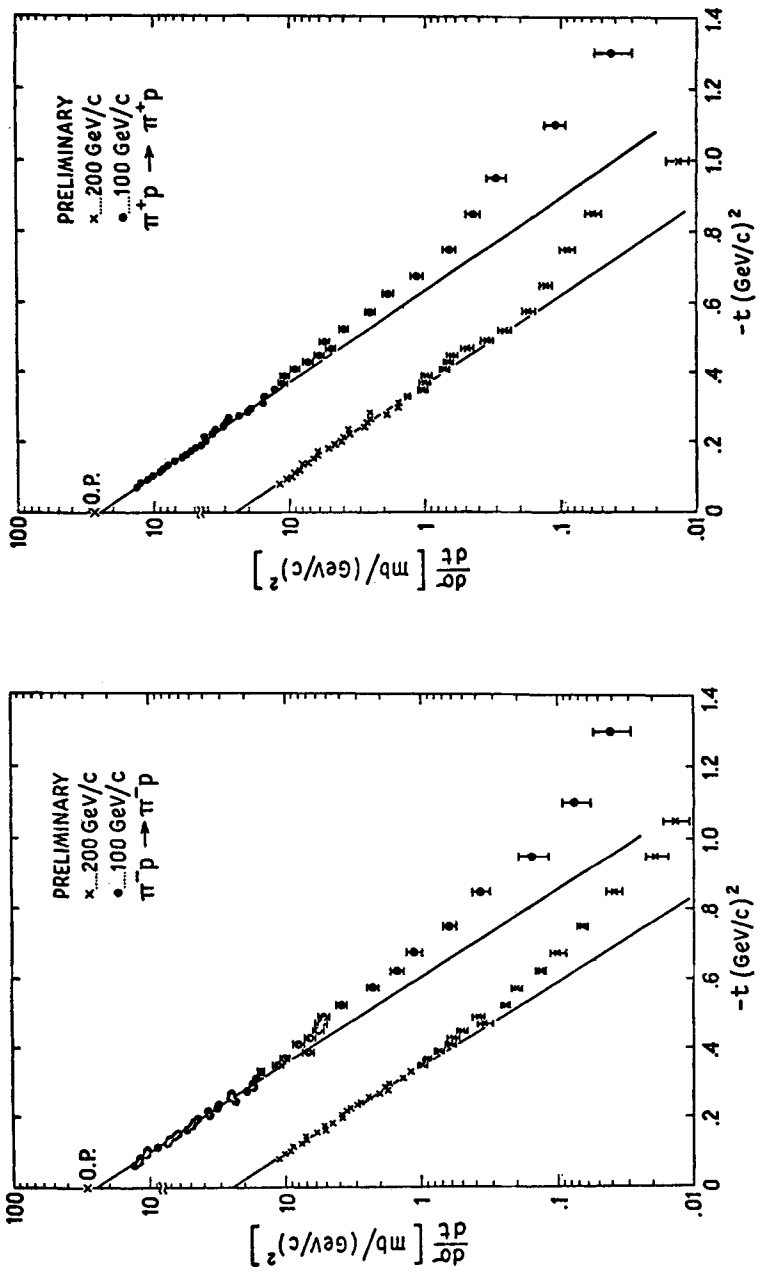


Fig. 13: Elastic Differential Cross-section $\pi^{\pm}p$

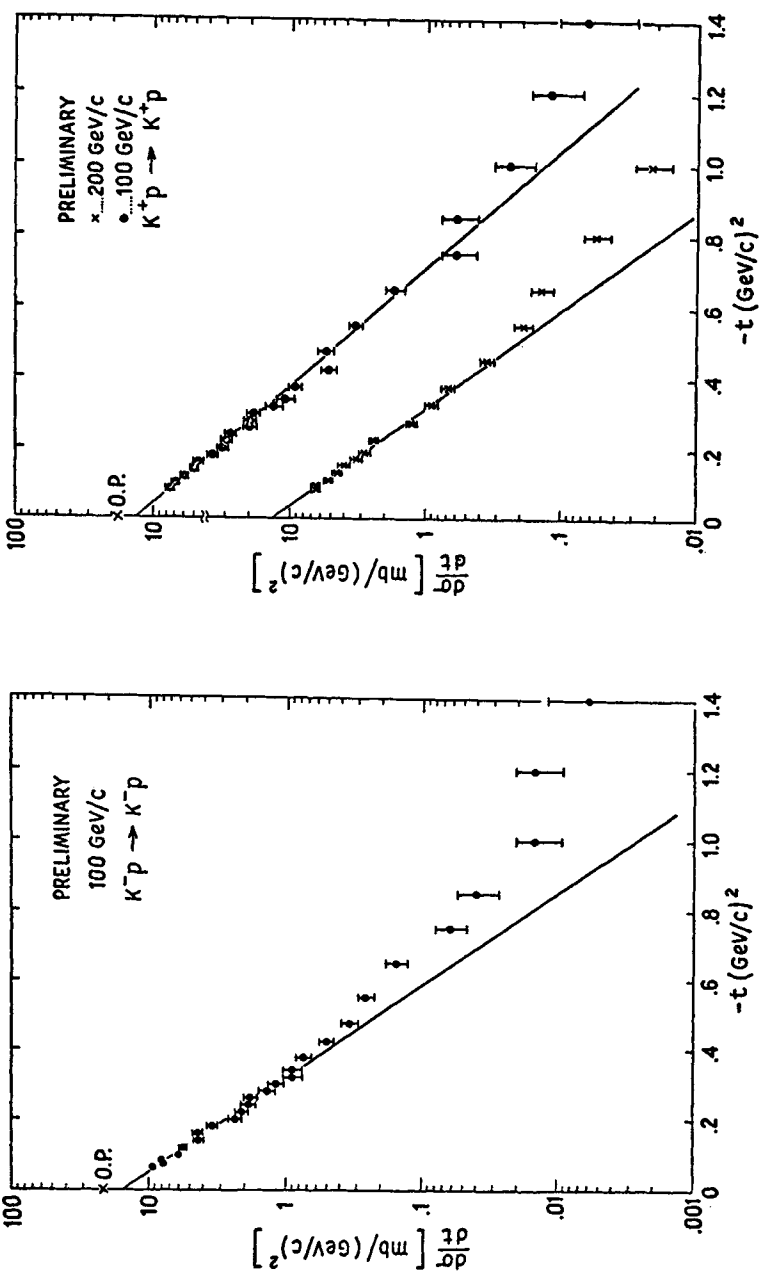


Fig. 14: Elastic Differential Cross-section $K^{\pm}p$

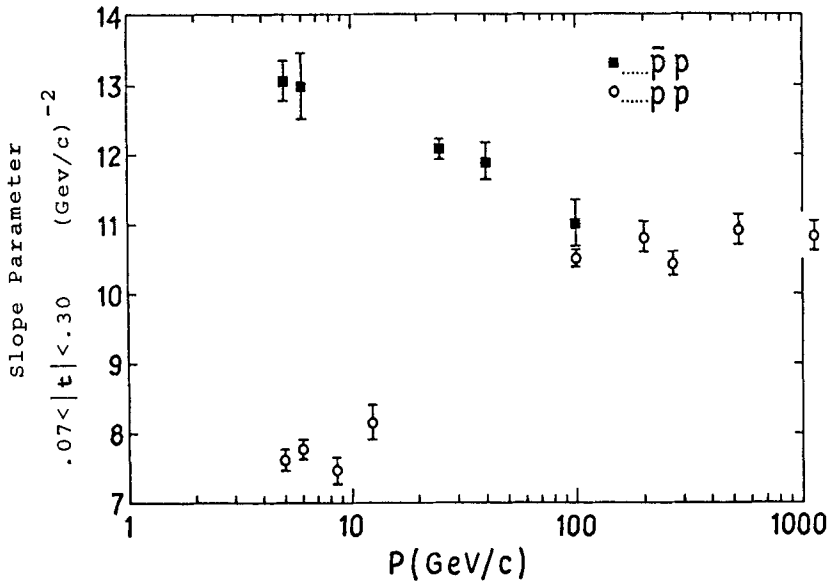


Fig. 15: Energy Dependence of Diffraction Slope $p^{\pm}p$

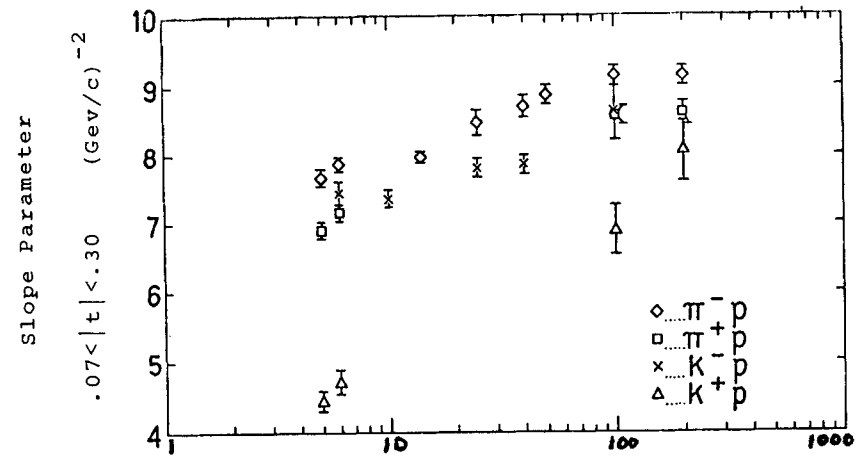


Fig. 16: Energy Dependence of Diffraction Slope $\pi^{\pm}p$ and $K^{\pm}p$

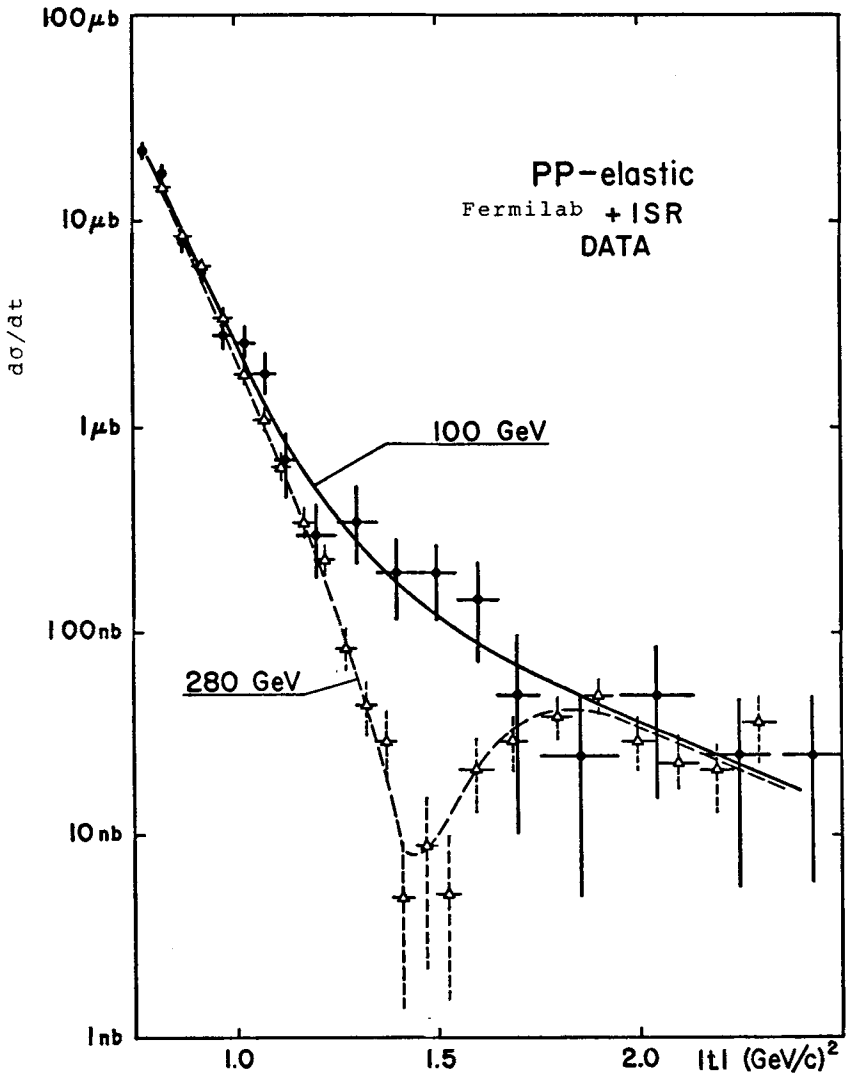


Fig. 17: Elastic Differential Cross-section for pp near $|t| \sim 1.4$ $(GeV/c)^2$: the Dip Region.